Rapid Communications

$Fe_4Nb_2O_9$: A magnetoelectric antiferromagnet

Antoine Maignan* and Christine Martin

CRISMAT, Laboratoire de Cristallographie et Sciences des Matériaux, UMR6508, Normandie Université, ENSICAEN, UNICAEN, CNRS, CRISMAT, 14000 Caen, France

(Received 26 February 2018; published 9 April 2018)

The structural, magnetic, and electrical properties of a $Fe_4Nb_2O_9$ polycrystalline sample have been characterized. It is found that this compound crystallizes in the $P\bar{3}c1$ space group of the α-Al_2O_3 structure and is thus isostructural to $Co_4Nb_2O_9$ and $Mn_4Nb_2O_9$, two linear magnetoelectric oxides. But in marked contrast, its $\varepsilon'(T)$ curve reveals two broad transitions at $T_{N1} \cong 90$ K and $T_{N2} \cong 77$ K, the former corresponding to the antiferromagnetic ordering temperature. Below T_{N1}, the $M(H)$ magnetization curves reveal the existence of spin flop at about 6 T. In this temperature region, a H-induced electric polarization for $\mu_0 H > 6$ T is evidenced by both sets of $I_p(T)_H$ and $P(H)_T$ curves. All these results point towards $Fe_4Nb_2O_9$ being a magnetoelectric member of the $A_4B_2O_9$ family (A = Mn, Fe, Co and B = Nb, Ta).

DOI: 10.1103/PhysRevB.97.161106

Multiferroic materials exhibiting at least two ferroic orders such as ferroelectricity and ferromagnetism are the focus of researchers' attention [1]. The magnetoelectric coupling is very appealing for applications in devices such as memories, where the magnetic information has to be controlled by an electric field. From the fundamental point of view, the coexistence of antagonist properties—ferroelectric and magnetic orders—has been boosted by reports on spin driven (or type-II) multiferroics (MF) in which the magnetic ordering is responsible for the breaking of the inversion symmetry; i.e., $T_C \leqslant T_N$ [2]. For this MF class, as noncollinear antiferromagnetic structures are looked for, most of the candidates exhibit frustrated magnetic networks, with low magnetic ordering temperatures, as in delafossites [3]. However, some oxides make exceptions, such as CuO tenorite [4], "112" $YBaCuFeO_5$ [5], or hexaferrites [6]; room-temperature (RT) magnetoelectric (ME) coupling is exhibited for some of them [7].

In addition to this type-II MF system, there exists another class of spin-induced ferroelectrics linked to the so-called linear ME (LME) effect (Ref. [8], and references therein). These compounds also crystallize in centrosymmetric structures, but exhibit collinear antiferromagnetic structures, and their electric polarization (P) is not spontaneous but is induced by applying an external magnetic field (H) and increases linearly with H. Indeed, their magnetic point group breaks both the inversion and time-reversal symmetries authorizing a diagonal LME effect to develop as $H > H_{\text{spin-flop}}$. The space groups authorizing such effects being scarce, the number of such materials is limited: Cr_2O_3 crystallizing in a corundum structure is a long-known example of LME [9,10] and, more recently, $Co_4Nb_2O_9$ and $Mn_4Nb_2O_9$ were reported to also belong to the LME class [11,12]. They both crystallize in the $P\bar{3}c1$ trigonal centrosymmetric structure [Fig. 1(a)] derived from the α-Cr_2O_3 corundum one.

Although their magnetic structures are still debated, with two proposed magnetic points, $\bar{3}m'$ or $c2/c'$, for $Co_4Nb_2O_9$ [13,14], the interesting LME properties reported for $Mn_4Nb_2O_9$ and $Co_4Nb_2O_9$ [11,12,14–16], containing $3d^5$ Mn^{2+} and $3d^7$ Co^{2+} magnetic cations, respectively, motivated us to study the $3d^6$ Fe^{2+} isotype oxide [17,18].

In this Rapid Communication, we report on the investigation of the structural, magnetic, dielectric, and ferroelectric properties of polycrystalline $Fe_4Nb_2O_9$. It exhibits (i) an intermediate $T_N (\cong 90$ K) between $T_N = 28$ K for $Co_4Nb_2O_9$ [13] and $T_N = 109$ K for $Mn_4Nb_2O_9$ [12], (ii) two spontaneous dielectric anomalies at 90 and 77 K on the $\varepsilon'(T)$ curve, and (iii) a H-induced electric polarization below T_N for $\mu_0 H > 6$ T. All these results point towards $Fe_4Nb_2O_9$ being a ME member of the $A_4B_2O_9$ family (A = Mn, Fe, Co and B = Nb, Ta).

The $Fe_4Nb_2O_9$ polycrystalline sample was synthetized by solid-state reaction. Fe, Fe_2O_3, and Nb_2O_5 precursors were weighted in order to respect the 4:2:9 nominal ratio. After grinding in an agate mortar, 1 g of powder was pelletized in bars of $2 \times 2 \times 10$ mm dimension which were sealed under primary vacuum in a closed ampoule, to be heated at 1100 °C for 6 h. Small, thin platelets ($2 \times 2 \times 0.5$ mm) were obtained by cutting the obtained bars perpendicularly to their long axis. Silver paste was deposited on the two 2×2 mm larger surfaces to attach electric copper wires for dielectric and pyroelectric measurements. The sample was soldered to a homemade sample probe which is inserted in a 14T-PPMS (Quantum Design). The dielectric permittivity is obtained using an Agilent 4284A LCR meter. An electrometer was used for pyroelectric current collection. The magnetic characterizations were performed using either a SQUID magnetometer (Quantum Design) for T-dependent magnetic moment measurements [zfc and fc are for zero-field cooling and field cooling, respectively (10^{-2} T)] or the ACMS option of the 14T-PPMS for H-dependent ones.

The purity of the phases was checked using room-temperature x-ray powder diffraction (XRPD) using a PANalytical diffractometer (Co $K\alpha$ radiations). The structural refinements in the $P\bar{3}c1$ space group of the α-Al_2O_3 [Fig. 1(b)]

*antoine.maignan@ensicaen.fr

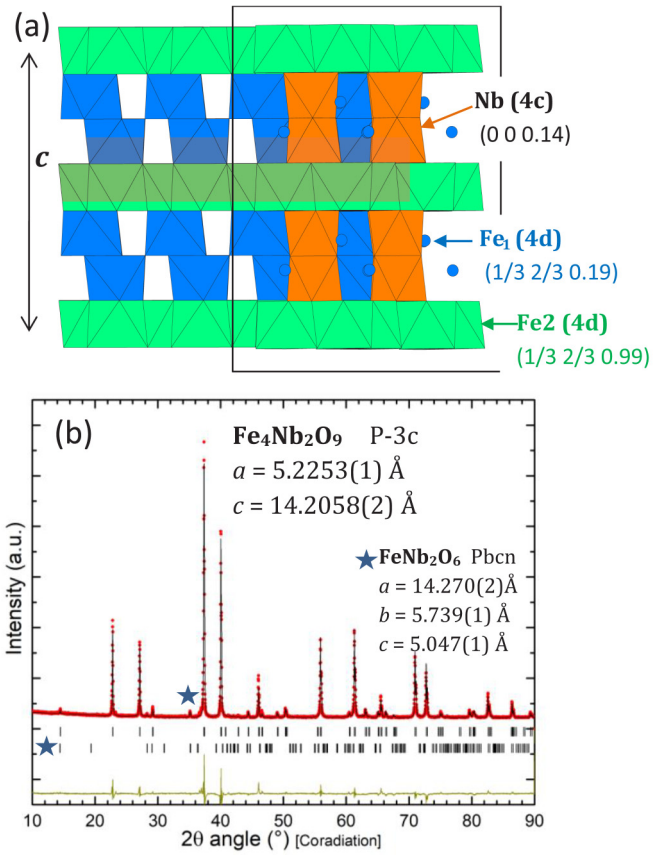

FIG. 1. (a) Schematic structure of $Fe_4Nb_2O_9$ (only the FeO_6 octahedra are shown in the left and the NbO_6 octahedra are added in the right part). (b) RT XRPD pattern. The points and lines correspond to the experimental data and calculated pattern, respectively. The vertical ticks correspond to the Bragg positions of the majority ($Fe_4Nb_2O_9$) and minority ($FeNb_2O_6$ denoted by a star) phases calculated in $P\bar{3}c1$ and *Pbcn* space groups, respectively. The corresponding sets of refined unit-cell parameters are also given.

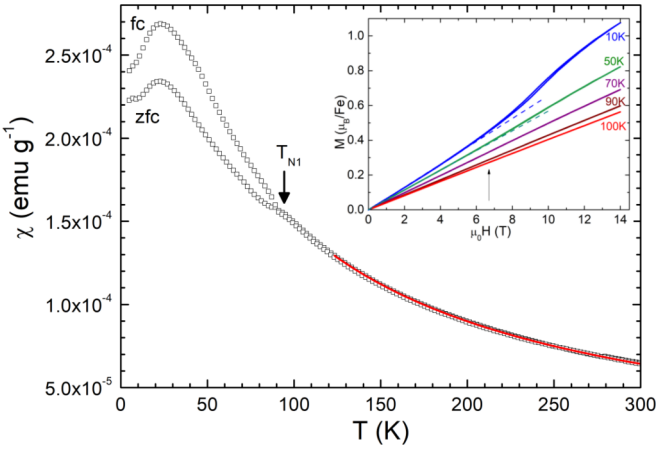

FIG. 2. T dependence of the magnetic susceptibility (χ) measured at 10^{-2} T. The Néel temperature is also indicated by an arrow. The curve superimposed over the data points corresponds to the Curie-Weiss fitting in the 120–300 K region. Inset: isothermal H-dependent magnetization (M) collected at different T for $\mu_0 H$ up to 14 T. The vertical arrow indicates the $\mu_0 H$ region of the spin-flop transition near 6 T. The dashed lines are guides to the eyes to visualize the $M(H)$ deviation from linearity.

show that the main phase is characteristic of $Fe_4Nb_2O_9$, with $a = 5.2253(1)$ Å and $c = 14.2058(2)$ Å [$V = 335.912(3)$ Å^3]. A small amount of $FeNb_2O_6$ is also detected [Fig. 1(b)] in a quantity estimated lower than 2% as previously reported [19]. As $T_N = 4.6$ K for $FeNb_2O_6$ [19] and as the measurements were all performed at 5 K and above, the observed transitions in the present study could not be ascribed to this secondary phase.

The curve of magnetic susceptibility (χ) as a function of temperature (Fig. 2) leads to $T_N \cong 90$ K for $Fe_4Nb_2O_9$ to be compared to $T_N \cong 28$ K for the Co-based sample [13,14,16]. Below T_N, the zero-field-cooling (zfc) and field-cooling (fc) curves start to diverge and then go through a maximum at about 25 K. The $\chi(T)$ curve was fitted with a Curie-Weiss law, $\chi = C/(T + \theta)$ for 120 K $\leqslant T \leqslant$ 300 K (Fig. 2). This leads to $\theta_p = -51$ K which indicates that antiferromagnetic (AF) interactions dominate and to $\mu_{\text{eff}} = 5.0\mu_B$/Fe, in good agreement with $\mu_{\text{eff}} = 4.9\ \mu_B$ expected for high-spin $3d^6$ Fe^{2+}, consistent with the Nb^{5+} and O^{2-} oxidation states.

As a spin flop was reported for $Co_4Nb_2O_9$ below T_N [13–16], a series of isothermal H-dependent magnetization curves [$M(H)$] was registered (inset of Fig. 2). At $T = 10$ K, the maximal M value in 14 T corresponds to $1.08\mu_B$/Fe which remains far from the theoretical one [Fe^{2+} ($S = 2$) : $4\mu_B$/Fe]. For $T \leqslant 50$ K, a clear deviation from linearity is detected in the $M(H)$ curves above 6 T, in particular at 10 K, which suggests the beginning of a spin flop. Although a spin-flop transition is of first order, our data collected for a polycrystalline sample might explain the smearing out of the transition.

To check for a possible magnetodielectric (MDE) coupling, the temperature dependence of the dielectric permittivity [$\varepsilon'(T)_f$] was collected (Fig. 3). These curves recorded upon heating reveal two transitions taken at $T_{N1} \cong 90$ K and $T_{N2} \cong$

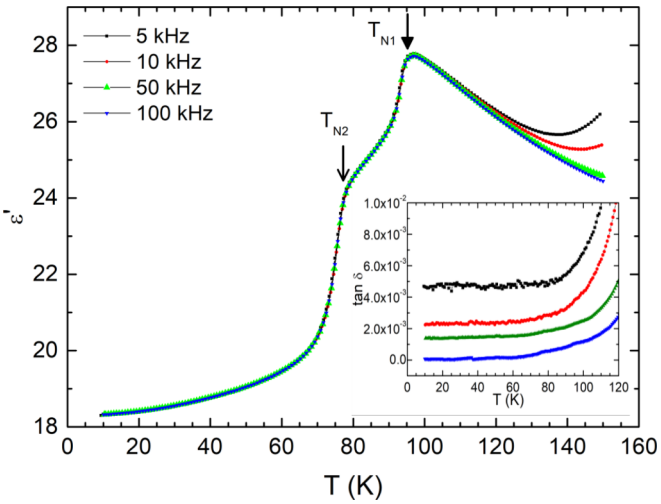

FIG. 3. ε' as a function of T collected at different frequencies ($f = 5$, 10, 50, 100 kHz). Inset: losses ($\tan\delta$) as a function of T for the same f; T_N values are labeled in the graph.

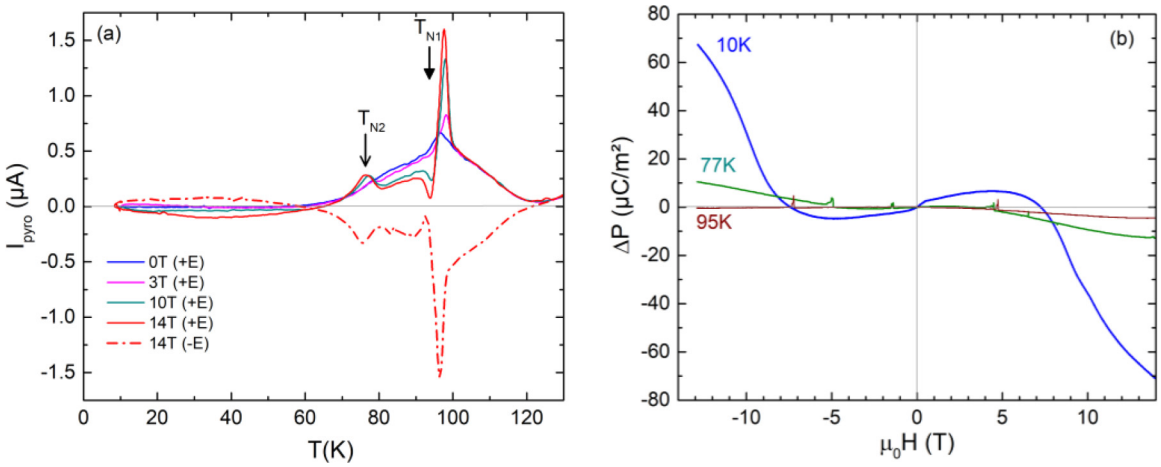

FIG. 4. (a) Curves of the pyroelectric current (I_p) as a function of T collected at different H after a magnetoelectric poling. Reversing E leads to opposite values of I_p. On these curves, two peaks are induced by the largest H at temperatures near to T_{N1} and T_{N2}. $E = \pm 87\,\mathrm{kV\,m^{-1}}$. (b) Isothermal H dependence of relative change of the electric polarization (ΔP). T values are labeled in the graph.

77 K. Thus, T_{N1} corresponds to T_N determined from the $\chi(T)$ curve (Fig. 2). In contrast, the transition at "T_{N2}" cannot be detected on the $\chi(T)$ curve, and thus cannot be attributed to a long-range order magnetic transition but rather indicate a spin reorientation or even a structural transition. The ε' changes at T_{N1} and T_{N2} are huge (Fig. 3), from $\varepsilon' = 28$ down to $\varepsilon' = 25$ at T_{N1} and then from $\varepsilon' = 25$ to about $\varepsilon' = 20$ at T_{N2} corresponding thus to a total change $\Delta\varepsilon'/\varepsilon'$ of nearly 30%. Moreover, the lack of frequency dependence supports an intrinsic origin. This temperature dependence of ε' differs from those reported for $Co_4Nb_2O_9$ [20] and $Mn_4Nb_2O_9$ [12] as for both oxides, in the absence of a magnetic field, the $\varepsilon'(T)$ curves exhibit no special feature at their unique AF transition temperature. In $Fe_4Nb_2O_9$, for $T > 110$ K, the $\varepsilon'(T)_f$ curves start to diverge which is explained by the beginning of the losses as shown in the inset of Fig. 3. A similar feature was reported for $Co_4Nb_2O_9$ [20] but not for $Mn_4Nb_2O_9$ [12]. Thus, in contrast to both $Mn_4Nb_2O_9$ and $Co_4Nb_2O_9$, which in the absence of an external magnetic field application do not exhibit an anomaly at T_N, $Fe_4Nb_2O_9$ exhibits large ε' variations. For the Mn_4 and Co_4 members, an external magnetic field application is needed to induce a ε' peak at T_N whose maximal value increases with H leading to positive magnetodielectric effects of 0.17% in $Mn_4Nb_2O_9$ in 12 T [12] and 11% in $Co_4Nb_2O_9$ in 9 T [20]. For these compounds, the MDE is consistent with the observed LME effect; i.e., there is no spontaneous electrical polarization ($P = 0$ for $\mu_0 H = 0$) and P is proportional to H.

The integration of a pyroelectric current to look for a LME effect requires a ME poling (H, E) prior to warming within H of a value larger than the field needed for the spin-flop transition. The T dependence of the pyroelectric current (I_p) collected in a magnetic field H upon warming after the ME poling (14 T, $E = +87\,\mathrm{kV\,m^{-1}}$) is given in Fig. 4(a). This ME poling consists of applying E and 14 T ($H_\perp E$) at 120 K prior to cooling down to 10 K. At that temperature, E is set at 0 and H at the value used for the measurements. After a waiting time of 5400 s, the $I_p(T)$ measurements are taken upon warming at $4\,\mathrm{K\,min^{-1}}$. For $\mu_0 H > 6$ T, these curves reveal two peaks, a smaller one at T_{N2} and a larger one at T_{N1}. For $\mu_0 H < 6$ T, these peaks are hardly discernible [0 and 3 T in Fig. 4(a)]. Furthermore, reversing E to $E = -87\,\mathrm{kV\,m^{-1}}$ switches the I_p values. Both features support the existence of H-induced polarization in magnetic fields larger than those needed for the spin flop. This is confirmed by collecting $I_p(H)$ curves at different temperatures, from which the H dependence of the electrical polarization is obtained [Fig. 4(b)]. These data were collected using the same type of ME poling down to the temperature of measurements. Decreasing $\mu_0 H$ from 14 T down to 0 T and then to −14 T leads to symmetric branches as expected for magnetoelectrics. At 10 K, the $\Delta P(H)$ curve evidences a H-induced P for $|\mu_0 H| > 6$ T in good agreement with the $I_p(T)$ curve of Fig. 4(a). One obtains a maximum for the ΔP induced by 14 T of $70\,\mu\mathrm{C\,m^{-2}}$ at 10 K. At $T = 10$ K, the comparison of the $\Delta P(H)$ and $M(H)$ (inset of Fig. 2) curves demonstrates the coupling between the spin flop and electrical polarization change for $|\mu_0 H| > 6$ T.

In conclusion, $Fe_4Nb_2O_9$, belonging to the honeycomb antiferromagnet $A_4B_2O_9$ class of compounds, exhibits two transitions in its T-dependent dielectric permittivity, the highest one corresponding to the AF transition at $T_{N1} \cong 90$ K whereas the second one could be the signature for a spin reorientation or a structural transition. These changes correspond to a 30% total variation of ε'. Such variations are not observed in either $Co_4Nb_2O_9$ [20] or $Mn_4Nb_2O_9$ [12] whose dielectric permittivity changes are only induced under magnetic field application. Another major difference is related to the spin-flop magnetic field H_{sf}, with $\mu_0 H_{sf} = 0.2$ T in $Co_4Nb_2O_9$ [15] as compared to the much higher $\mu_0 H_{sf}$ value close to 6 T found in $Fe_4Nb_2O_9$. This is probably related to the a stronger Fe^{2+}-O - Fe^{2+} superexchange pathway in the Fe-honeycomb layer in the (a,b) plane of the structure [sheet of green Fe polyhedra in Fig. 1(a)]. By comparing the $I_p(T)_H$ curves obtained after a ME poling, it is clear that a H induces a polarization for $H > H_{sf}$ which is confirmed by the $\Delta P(H)_T$ curves. From this first set of characterizations, it is concluded that $Fe_4Nb_2O_9$ is ME but additional experiments are now needed to establish the magnetic structure(s) and to understand the origin of the transitions observed in the dielectric permittivity. Measurements on crystals would also be required to quantify

the electric polarization created by applying a magnetic field along the different crystallographic directions of the corundum structure to reveal the presence or absence of a ferrotoroidic order as in $Co_4Nb_2O_9$ [16].

[1] Y. Tokura, S. Seki, and N. Nagaosa, Rep. Prog. Phys. **77**, 076501 (2014).

[2] D. Khomskii, Physics **2**, 20 (2009).

[3] S. Seki, Y. Onose, and Y. Tokura, Phys. Rev. Lett. **101**, 067204 (2008).

[4] T. Kimura, Y. Sekio, H. Nakamura, T. Siegrist, and A. P. Ramirez, Nat. Mater. **7**, 291 (2008).

[5] B. Kundys, A. Maignan, and Ch. Simon, Appl. Phys. Lett. **94**, 072506 (2009).

[6] T. Kimura, Annu. Rev. Condens. Matter Phys. **3**, 93 (2012).

[7] Y. Kitagawa, Y. Hiraoka, T. Honda, T. Ishikura, H. Nakamura, and T. Kimura, Nat. Mater. **9**, 797 (2010).

[8] A.K. Agyei and J. L. Birman, J. Phys.: Condens. Matter **2**, 3007 (1990).

[9] I. E. Dzyaloshinskii, Zh. Eksp. Teor. Fiz. **37**, 881 (1959) [Sov. Phys. JETP **10**, 628 (1959)].

[10] D.N. Astrov, Zh. Eksp. Teor. Fiz. **38**, 984 (1960) [Sov. Phys. JETP **11**, 708 (1960)].

[11] E. Fischer, G. Gorodetsky, and R. M. Hornreich, Solid State Commun. **10**, 1127 (1972).

[12] Y. Fang, W. P. Zhou, S. M. Yan, R. Bai, Z. H. Qian, Q. Y. Xu, D. H. Wang, and Y. W. Du, J. Appl. Phys. **117**, 17B712 (2015).

[13] E. F. Bertaut, L. Corliss, F. Forrat, R. Aleonard, and R. Pauthenet, J. Phys. Chem. Solids **21**, 234 (1961).

[14] N. D. Khanh, N. Abe, H. Sagayama, A. Nakao, T. Hanashima, R. Kiyanagi, Y. Tokunaga, and T. Arima, Phys. Rev. B **93**, 075117 (2016).

[15] Y. Fang, Y. Q. Song, W. P. Zhou, R. Zhao, R. Zhao, R. J. Tang, H. Yang, L. Y. Lv, S. G. Yang, D. H. Wang, and Y. W. Du, Sci. Rep. **4**, 3860 (2014).

[16] N. D. Khanh, N. Abe, S. Kimura, Y. Tokunaga, and T. Arima, Phys. Rev. B **96**, 094434 (2017).

[17] A. Burdese and M. Lucco Borlera, Metall. Ital. **57**, 150 (1965).

[18] K. Kitayama, J. Solid State Chem. **69**, 101 (1987).

[19] P. W. C. Sarvezuk, E. J. Kinast, C. V. Colin, M. A. Gusmao, J. B. M. da Cunha, and O. Isnard, Phys. Rev. B **83**, 174412 (2011).

[20] T. Kolodiazhnyi, H. Sakurai, and N. Vittayakorn, App. Phys. Lett. **99**, 132906 (2011).